Electron relaxation by LO phonons in quantum wires: An adiabatic approach

C. Ammann
Institute of Theoretical Physics, University of Lausanne, CH-1015 Lausanne, Switzerland

M. A. Dupertuis
Institute of Micro- and Optoelectronics, Department of Physics, Swiss Federal Institute of Technology, CH-1015 Lausanne, Switzerland

U. Bockelmann
Walter Schottky Institut, Technische Universität München, D-85748 Garching, Germany

B. Deveaud
Institute of Micro- and Optoelectronics, Department of Physics, Swiss Federal Institute of Technology, CH-1015 Lausanne, Switzerland
(Received 7 June 1996; revised manuscript received 3 September 1996)

The electron states of weakly-one-dimensional quantum wires are computed using the adiabatic approximation in the framework of the $\mathbf{k}\cdot\mathbf{p}$ theory and the envelope-function approximation. The computed transition rates of electrons from one confined state to any other, mediated by the longitudinal optical (LO) phonons, are clearly ordered with respect to the quantum numbers of the states provided by the adiabatic approximation. The average single electron relaxation time from an excited level is shown to either increase or surprisingly decrease as a function of initial energy. Finally, the relaxation dynamics of an excited population of electrons is analyzed. We show that a fast phenomenological intrasubband thermalization, simultaneous to the LO phonon-mediated relaxation, lowers the final average energy and may in some cases significantly speed up the whole relaxation. [S0163-1829(97)07004-5]

I. INTRODUCTION

A principal axis of research on electronic devices relies on the inclusion of low-dimensional semiconductor heterostructures, because of their potential ability to tailor the electronic states and the electronic phase space. Such possibilities were recognized long ago, but it is only recently that the technology has begun to deliver quality structures suitable for conclusive experimentation. In the fields of both electronics (transport) and optics, faster and more economic devices may be expected.[1,2] Such features partly result from reduced or enhanced carrier scattering rates.

In typical optical experiments, the excited charge carriers (electrons and holes) relax to the bottom of their respective bands before they recombine, since the radiative recombination is a slow process ($\sim$350 ps) (Ref. 3) obeying k-selection rules. Many processes contribute to the relaxation (Coulomb interaction, impurity scattering, phonon emission, etc.). In quantum wires, longitudinal optical (LO) phonon emission is the most efficient one, while carrier-carrier Coulomb interaction is drastically reduced with respect to the bulk.[4–6]

Many specific theoretical studies of the mechanism of phonon emission in quantum wires are available.[4–34] Riddoch and Ridley[7] and Leburton[8] first considered relaxation by LO phonons in rectangular quantum wires. They readily showed the singularities which arise from the one-dimensional (1D) density of states. In later papers, Leburton showed that high carrier mobility can be achieved under electrical field[4,9,10] and that ''phonon pumping'' can induce an optical gain coefficient.[11,12] He also emphasized that LO phonons maintain nonthermal charge carrier populations.[4]

Bockelmann and Bastard[13] compared LO and acoustic phonon scattering in rectangular structures of different dimensionality (2D, 1D, and 0D). They showed that the LO phonon 1D scattering rates and energy-loss rates oscillate around the 2D values as a function of the energy.

Many groups have studied the relevance of using bulk LO phonon dispersion relations for scattering rate computation in 1D structures instead of confined and interface optical phonons.[14–19] The conclusion reached by Jiang and Leburton[20] and confirmed by Rossi *et al.*[21] is that the scattering rates obtained using GaAs bulk LO phonons reproduce well those due to both confined and interface optical phonons for $Al_{\delta}Ga_{1-\delta}As$-GaAs wires of diameters exceeding 50 Å. Furthermore, polarons have been shown to be an irrelevant refinement for scattering rate calculations.[22] The effects of hot phonon saturation are more important[23,24] and reduce the cooling rate for high-density carriers.

The emission of acoustic phonons has also been extensively investigated[12,13,25–29] but, in that case, the scattering rates are about three orders of magnitude below the ones due to LO phonon interactions. However, the linear dispersion relation of acoustic phonons makes them necessary for low energy ($<\hbar\omega_{\mathrm{LO}}$) dissipation processes.

The purpose of the present work is to specify qualitatively as well as quantitatively the characteristic features of relaxation processes of electrons in realistic semiconductor quantum wires mediated by LO phonons. In order to classify the electron states in terms of quantum numbers and to obtain reasonable computing times, we have used an adiabatic model of the quantum wire.[30,31] Such a model is particularly suitable for ''weakly 1D'' structures,[31] i.e., heterostructures unconfined in some direction (translational symmetry),

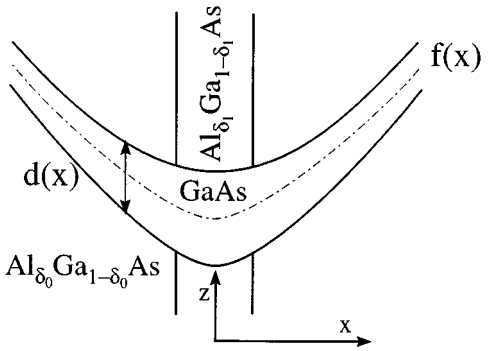

FIG. 1. Schematic section of a V-groove $Al_{\delta}Ga_{1-\delta}As$ quantum wire as an example of an adiabatic quantum wire. The vertical well (Al concentration $\delta_1 < \delta_0$) is present only in MOCVD grown wires.

strongly confined in another, and weakly confined in the last one. This approximation allows the dynamics to be investigated in detail, including excited states. To be as realistic as possible, the model types chosen are crescent-shaped quantum wires[30,32] or V-grooved quantum wires[3] which have been manufactured and studied experimentally. This study concentrates on the relaxation of electrons, disregarding holes and many-body interactions. This assumption restricts the applicability of our results to the cases where the electronic relaxation dominates, as in low-density electron injection experiments or situations in which large screening effects weaken the excitonic behavior.

Two Monte Carlo works are connected with the present paper. Vurgaftman and Singh[33] have studied the duration of electron relaxation in rectangular wires assisted by carrier-carrier and LO phonon-carrier interaction. Kiener *et al.*[34] have shown that capture processes from extended states to bound states of a specific V-grooved wire can be especially quick (a few ps).

Figure 1 shows an example of the cross section of a quantum wire described by our theoretical approach. Such structures can be grown on V-grooved GaAs substrates either by metal organic chemical vapor deposition (MOCVD)[30,32] or by molecular beam epitaxy (MBE).[3] The quantum wire consists of the GaAs potential well surrounded by $Al_{\delta}Ga_{1-\delta}As$ barriers. Along the growth axis z, the quantum wire is in the range 5–30 nm thick in the central region ($x=0$) and becomes thinner on the sides. Its characteristic lateral width is typically five to ten times larger. The barriers of MOCVD structures usually contain a two-dimensional vertical well of low Al concentration δ_1 corresponding to a potential well whose depth is between those of the wire and the barriers (Fig. 1).

We use the envelope-function approximation and the adiabatic approximation to describe the electronic states. The rates of electronic transitions mediated by optical phonons between the compatible bound states of the conduction band are computed using the Fermi golden rule. These data are collected to describe the dynamics of cooling in adiabatic quantum wires. This approach simplifies the computation in order to give a deeper insight into the physics.

II. THEORY

The quantum wire cross section is described by the z position of its center $z=f(x)$ (dot-dashed line on Fig. 1) and its half-width $d(x)$. The effective mass $m^*(x,z)$ and the potential $V(x,z)$ experienced by the conduction electrons are steplike functions, whose values increase with the Al concentration δ of each domain. In the effective mass approximation, the envelope wave functions along y are plane waves (of wave vector $k_y \equiv k$) as a result of translational invariance, and the Schrödinger equation for the conduction band electrons becomes two-dimensional,

$$H\psi_k(x,z)=\left\{-\frac{\hbar^2}{2}\nabla\frac{1}{m^*(x,z)}\nabla+\frac{\hbar^2k^2}{2m^*(x,z)}+V(x,z)\right\}\times\psi_k(x,z)=E_k\psi_k(x,z) \quad , \tag{1}$$

where ∇ is the two-dimensional gradient operator, $\psi_k(x,z)$ the two-dimensional wave function, and E_k the eigenenergy of the electron. One approach consists in diagonalizing the Hamiltonian H numerically. The adiabatic method presented in the following has two major qualities: it is numerically simple to handle and it classifies the wave functions naturally in terms of two quantum numbers. This classification gives indications on how to interpret the results, as will be shown in Sec. III.

A. Adiabatic approximation

The adiabatic approximation only applies to structures with smooth $f(x)$ and $d(x)$. The wave function is quasifactorized in $\psi_k(x,z)=\phi_k(x)\chi_k^x(z)$ and the effective mass Hamiltonian is divided into an operator H_{L}, local in x, plus a nonlocal one, H_{NL}, including all the x derivatives. The local operator acts only on $\chi_k^x(z)$. Its eigenvalues $V_{k,m}^{\mathrm{eff}}(x)$ and eigenfunctions $\chi_{k,m}^x(z)$ are solutions of

$$H_{\mathrm{L}}\ \chi_k^x(z)=\left\{-\frac{\hbar^2}{2}\partial_z\frac{1}{m^*(x,z)}\partial_z+\frac{\hbar^2k^2}{2m^*(x,z)}+V(x,z)\right\}\times\chi_k^x(z)=V_k^{\mathrm{eff}}(x)\chi_k^x(z) \quad , \tag{2}$$

with x treated as a parameter. Equation (2) is that of an electron in a one-dimensional potential well given by $\hbar^2k^2/2m^*(x,z)+V(x,z)$ and its solutions are a set of Ben-Daniel-Duke wave functions numbered by the z quantum number m.[35]. Inserting the right-hand side (rhs) of Eq. (2) into Eq. (1) gives the 1D Schrödinger equation for an effective potential $V_k^{\mathrm{eff}}(x)$ along x (Fig. 2) acting on $\phi_k(x)$,

$$\left\{-\frac{\hbar^2}{2}\partial_x\frac{1}{m_{k,m}(x)}\partial_x+V_{k,m}^{\mathrm{eff}}(x)\right\}\phi_k(x)=E_k\phi_k(x) \quad . \tag{3}$$

At $k=0$, the final eigenvalues $E_{k,m,i}$, where i is the x quantum number, are edges of 1D subbands. In Eq. (3), $m_{k,m}(x)$ is a ponderated reduced mass given by[35]

$$m_{k,m}^{-1}(x)=m_{\mathrm{GaAs}}^{-1}\int_{\mathcal{D}(\mathrm{GaAs})}dz|\chi_{k,m}^x(z)|^2+m_{\mathrm{Al}_{\delta}\mathrm{Ga}_{1-\delta}\mathrm{As}}^{-1}\int_{\mathcal{D}(\mathrm{Al}_{\delta}\mathrm{Ga}_{1-\delta}\mathrm{As})}dz|\chi_{k,m}^x(z)|^2 \quad . \tag{4}$$

$\mathcal{D}(\mathrm{GaAs})$ [$\mathcal{D}(\mathrm{Al}_{\delta}\mathrm{Ga}_{1-\delta}\mathrm{As})$] stands for the one-dimensional domain at x, along a line parallel to the z axis, where the effective mass equals a constant m_{GaAs} ($m_{\mathrm{Al}_{\delta}\mathrm{Ga}_{1-\delta}\mathrm{As}}$).

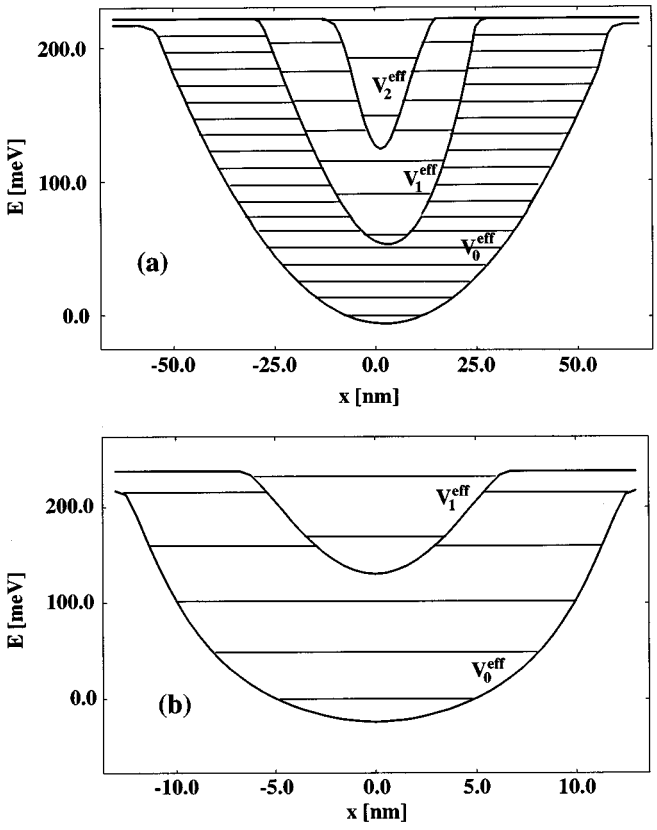

FIG. 2. Lateral electronic effective potentials $V^{\text{eff}}_{k=0,m}(x)$. The corresponding eigenvalues $E_{k=0,m,i}$ (subband edges) are displayed as horizontal bars. The two graphs (a) and (b) refer to two different quantum wires (large and small). In the two cases the origin of the energies is the ground subband edge $E_{00}=0.0$ meV.

In the Appendix we show analytically that the parabolic dispersion along y is governed by a ponderated effective mass m_{mi} which reads

$$m_{mi}^{-1}=\int dx\ m^{-1}_{k=0,m}(x)\left|\phi_{k=0,m,i}(x)\right|^2 \quad . \tag{5}$$

We checked that m_{mi} obtained in this way is perfectly consistent with the dispersion of the numerical solutions with $k\neq 0$ in the vicinity of $k=0$. In the following we shall, therefore, treat only the point $k=0$ and drop the k subscript. It should be noticed that this corresponds to making an approximation of k-independent phonon matrix elements since all wave functions $\psi_k(x,z)$ are evaluated at $k=0$.

The effective potentials $V^{\text{eff}}(x)$ are plotted in Figs. 2(a) and 2(b) for the two types of quantum wires studied. In case (a), typical of the structures grown by MBE,[3] the wire is fairly large and has a thickness of about 20 nm (at $x=0$): three values of the z quantum number m are possible. In (b), typical of structures grown by MOCVD,[30,32] the wire is thinner ($\simeq 7$ nm) and m equals 0 or 1. The horizontal lines identify the subband edges $E_{m,i}$. The origin of the energies is defined at $E_{m=0,i=0}=0.0$ meV. The confinement width of any subband $\{m,i\}$ is defined as the difference between the abscissas of both sides of $V^{\text{eff}}_m(x)$ at energy $E_{m,i}$.

The adiabatic approximation is reliable when the nature of the wave function $\chi^x(z)$ does not vary too much with x.[36] The presence of a vertical well (see Fig. 1) induces a rapid variation of the barrier potential along x. However, since the ratio of the barrier concentrations δ_1/δ_0 is larger than 90%, the vertical well is shallow. We have verified that the eigenenergies and wave functions are only slightly perturbed by the fact that $\delta_1/\delta_0\neq 1$.

B. Fermi golden rule

In this work the electronic transitions are mediated by longitudinal optical phonons since this is the most efficient of the various possible relaxation processes (impurity scattering, acoustic phonon scattering, carrier-carrier interactions, etc.). We assume that the LO phonons are not affected by the wire and have the characteristics of dispersionless bulk GaAs LO phonons as suggested by the sufficiently large thickness of the quantum wire.[21]

In the following, the basis states $|s\rangle$ of the electron-phonon system are denoted by three quantum numbers for the electron and by an occupation number set (in a Fock space) for the phonons

$$|s\rangle=|m,i,k\rangle\otimes|\{n_q\}\rangle. \tag{6}$$

The energy of these bare states is

$$E^{e\text{-ph}}=E_{m,i}+\frac{\hbar^2k^2}{2\,m_{mi}}+\sum_q\ n_q\hbar\omega_{\text{LO}}\quad , \tag{7}$$

where $\hbar\omega_{\text{LO}}$ is the energy of the dispersionless optical phonons.

The interaction between electrons and longitudinal optical phonons in polar crystals is the electric dipolar interaction, which can be described by the Fröhlich Hamiltonian

$$H_F=i\alpha\sum_q\ q^{-1}(a_qe^{iqr}-a_q^+e^{-iqr}) \tag{8}$$

with

$$\alpha=\left\{\frac{\hbar\omega_{\text{LO}}e^2}{2\epsilon_0V}[\epsilon_\infty^{-1}-\epsilon^{-1}(0)]\right\}^{1/2}, \tag{9}$$

where ϵ_∞ is the dielectric constant at infinite frequency, $\epsilon(0)$ the static dielectric constant, V is the global volume of the system, and a_q is the annihilation operator of a phonon of wave vector q. The Fermi golden rule gives the transition rate τ^{-1} of an electron from an initial state $|\text{in}\rangle$ to all the final ones $|\text{fi}\rangle$ in the framework of the first-order perturbation theory (first Born approximation), as

$$\tau^{-1}=\frac{2\pi}{\hbar}\sum_{|\text{fi}\rangle,q}\ \delta(E^{e\text{-ph}}_{\text{fi}}-E^{e\text{-ph}}_{\text{in}})\left|\langle\text{fi}|H_F|\text{in}\rangle\right|^2 \quad . \tag{10}$$

At low temperatures only phonon emission processes are of importance. Inserting the adiabatic electron wave functions $\psi_{k=0,m,i}(x,z)\exp(iky)$, we get the transition rate

$$\tau^{-1}=\sum_{k_{\text{fi}}}\ \tau^{-1}_{\text{in}\to\text{fi}}=\sum_{k_{\text{fi}}}\ \frac{V\alpha^2m_{\text{fi}}}{(2\pi)^2\hbar^3k_{\text{fi}}}\,(n_q+1)I_{\text{in}\to\text{fi}}(k_{\text{fi}}-k_{\text{in}}), \tag{11}$$

with $k_{\rm fi}$ determined by the requirement of energy conservation. The divergent prefactor $k_{\rm fi}^{-1}$ comes from the electronic density of states and is typical of 1D structures. The form factor $I_{\rm in\to fi}$ reads

$$I_{\rm in\to fi}(k_{\rm fi}-k_{\rm in})=\int\int dq_x dq_z |M_{\rm in\to fi}(q_x,k_{\rm fi}-k_{\rm in},q_z)|^2, \tag{12}$$

with the transition matrix element given by

$$M_{\rm in\to fi}(q_x,k_{\rm fi}-k_{\rm in},q_z) = |q|^{-1}\int dx \langle \chi^x_{m_{\rm fi}}|e^{-iq_z z}|\chi^x_{m_{\rm in}}\rangle \phi_{m_{\rm fi}i_{\rm fi}}(x)^* \times \phi_{m_{\rm in}i_{\rm in}}(x)e^{-iq_x x} \ . \tag{13}$$

The phonons are assumed to be in equilibrium and, hence, follow a Bose-Einstein distribution $n_q=(\exp(\hbar\omega_{\rm LO}/k_BT)-1)^{-1}$, where T is the lattice temperature.

III. RESULTS

To characterize the electronic relaxation by LO phonons in quantum wires, we first present results on the transitions rates between different pairs of quantum wire bound states in order to establish the dominant relaxation channels in Sec. III A. Such results will be used to interpret the calculation of the global average relaxation time of a single electron presented in Sec. III B. In Sec. III C, we analyze the relaxation dynamics of an excited electron population. The case of a large quantum wire with many subbands is compared with the case of a small quantum wire which provides much stronger confinement and fewer available states. Lastly, we introduce a fast simultaneous phenomenological intrasubband thermalization process.

A. Transition rates

Transition rates between different bound states of the wire are shown in Figs. 3 and 4 for the wire denoted by (a) in Fig. 2. The z quantum number $m_{\rm in}=1$ and x quantum number $i_{\rm in}=3$ refer to the subband of the initial states: for each value of the initial energy $E_{\rm in}$, the transition rate to every subband is evaluated using Eq. (11). The final subband z quantum number is $m_{\rm fi}=1$ in Fig. 3 and $m_{\rm fi}=0$ in Fig. 4. Both final subband quantum numbers $m_{\rm fi}$ and $i_{\rm fi}$ are marked along the curves.

It can be seen by comparison with Fig. 2(a) that divergences of the transition rate appear when the initial energy is $\hbar\omega_{\rm LO}$ above a subband edge. This comes from the one-dimensional density of the final states $|{\rm fi}\rangle$ in the expression for τ^{-1}. Such singularities can be avoided by introducing an energetic broadening of the states. However, this is deliberately omitted here to allow a precise resolution of the peaks. It can be added at a later stage for comparison with experimental data.

We see that intrasubband transitions ($m_{\rm fi}=m_{\rm in}$ and $i_{\rm fi}=i_{\rm in}$) are more probable than intersubband processes. This means that the electrons lose preferentially their longitudinal momentum (along y) before changing subbands, unless their kinetic energy is smaller than $\hbar\omega_{\rm LO}$ or if, accidentally, $E_{\rm in}$ is approximately $\hbar\omega_{\rm LO}$ above a subband edge. The duration of the relaxation through a definite channel is approximately the sum of the intersubband jumping times.

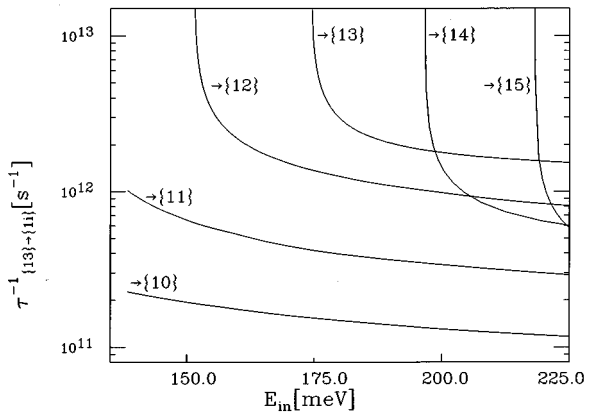

FIG. 3. LO-phonon scattering rates as a function of the initial energy of an electron placed in subband $\{m_{\rm in}=1,i_{\rm in}=3\}$ of the large quantum wire [Fig. 2(a)]. The z-quantum number $m_{\rm fi}$ of the final subbands is 1. Divergence happens $\hbar\omega_{\rm LO}$ above each final subband edge, due to the divergent 1D density of states. m-conserving transitions ($m_{\rm fi}=m_{\rm in}=1$) are ordered with respect to the x quantum number $i_{\rm fi}$, the maximum being reached for $i_{\rm fi}=i_{\rm in}=3$: intrasubband transition is the most probable (except for divergences).

It can be seen in Fig. 3 that the *lateral* transition rates, characterized by initial and final subbands with identical z

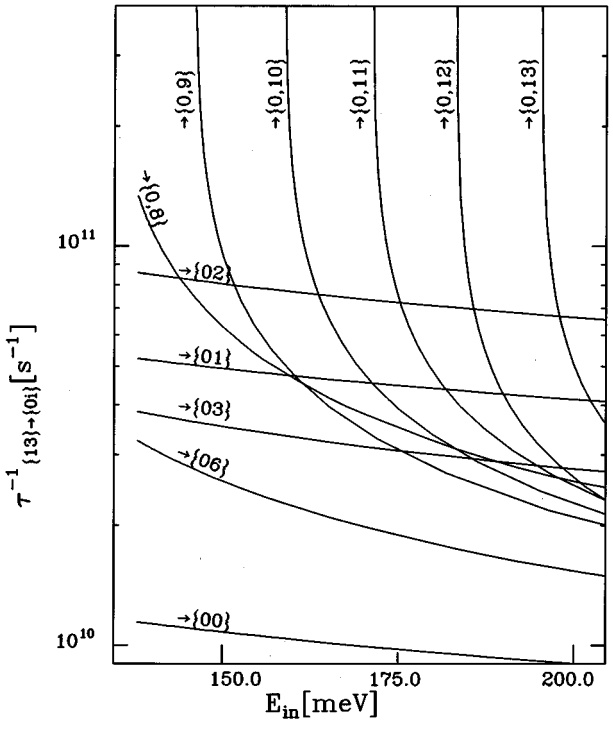

FIG. 4. LO-phonon scattering rates as a function of the initial energy of an electron placed in subband $\{m_{\rm in}=1,i_{\rm in}=3\}$ as in Fig. 3, but for transitions to states with a final quantum number $m_{\rm fi}=0$. The rates are much reduced with respect to Fig. 3 and are not well ordered, e.g., the transition rate towards state $\{0,2\}$ is higher than towards other states due to the fact that the wave functions have a larger overlap linked to ''more compatible'' peaks.

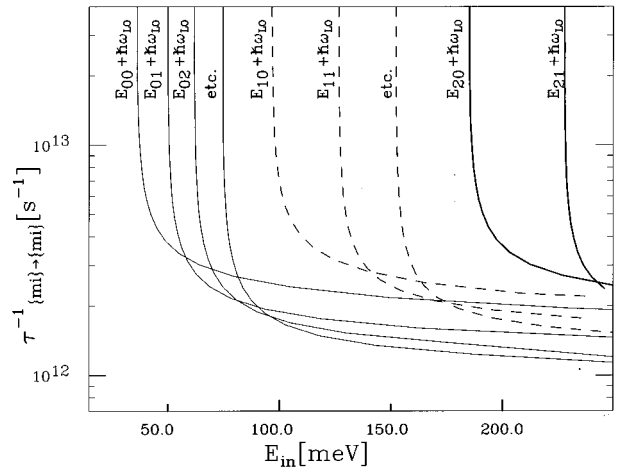

FIG. 5. Intrasubband transition rates for the subbands $\{m,i\}$ as a function of the initial energy. Thin-solid (dashed and thick-solid) curves refer to subbands with z-quantum number $m=0$ (1 and 2, respectively). The energy values at the divergences are indicated. The shift of the rate function when i increases is evident.

quantum numbers ($m_{\rm fi}=m_{\rm in}$), are well ordered in terms of $i_{\rm fi}$, in the sense that the relaxation rate function is shifted upwards as $i_{\rm fi}$ increases up to $i_{\rm fi}=i_{\rm in}$, and then downwards for higher values of $i_{\rm fi}$ (Fig. 3). This order, provided by the form factor $I_{\rm in\rightarrow fi}$, disappears for *mixed* transitions characterized by $m_{\rm fi}\neq m_{\rm in}$ (Fig. 4). Since the confinement width of the states along x varies with m [different $V_m^{\rm eff}(x)$ in Fig. 2], the overlap of the initial and final wave functions $\phi(x)$ may be very large and enhance the form factor $I_{\rm in\rightarrow fi}$. For example, the wave functions of states $\{1,3\}$ and $\{0,2\}$ have compatible peaks and, hence, the transition rate between them is particularly high (Fig. 4).

In Fig. 5, the intrasubband transition rates are presented for the first few subbands. The energy values of the divergences are indicated on the curves. For all subbands with the same m value, a hierarchy appears: the transition rate function shifts downward when i increases. This behavior is due to the fact that the operator $\exp(-iq_x x)$ in the matrix element $M_{\rm in\rightarrow fi}$ [Eq. (13)] acts as a translation operator on the rhs wave function $\phi_{m_{\rm in}i_{\rm in}}(x)$. The interference at small q_x becomes increasingly destructive with increasing x quantum number i.

Any quantitative comparison of our results with previous papers concerning rectangular[8,13,15,22] or cylindrical[37] geometries is made difficult due to the particular dimensions chosen by each author. While the confinement area of the states depends only weakly on the quantum numbers in rectangular or cylindrical wires, it is strongly affected by their values in the adiabatic wires. This can be seen in Fig. 2 (the confinement width along x varies with the quantum numbers). In adiabatic wires, the difference of the energies of two successive subband edges is nearly constant, contrary to that for rectangular or cylindrical quantum wires. If it matches a divisor of the LO phonon energy, resonance effects will speed up the relaxation.

The results concerning the quantum wire can be compared with corresponding calculations on quantum well structures.[38–41] Apart from the divergences due to the $1/\sqrt{E}$ peaks of the density of states, the mixed-transition scattering rates are smaller than intersubband rates in quantum wells, by factors varying from 15 up to 50 (Fig. 4). The intrasubband rates shown in Fig. 5 are two to six times smaller than intrasubband rates in the wells. The lateral transition rates (Fig. 3) lie between these two cases because they do not change the z quantum number. It is instructive to note that the sum of the lateral and intrasubband transition rates in quantum wires is quite comparable with the intrasubband transition rates in quantum wells. This order-of-magnitude analysis can be supplemented by two considerations: in a quantum wire, the transitions (intrasubband, lateral, or mixed) involve only a finite number of final states, instead of an infinity as in quantum wells, and this implies that the 1D relaxation rates will, in general, be smaller than in 2D structures; however, the momentum conservation rule has only to be applied in one direction in quantum wires instead of two in quantum wells, which weakens the preceding argument.

B. Average global relaxation time of a single electron

The lifetime of a state $\{m,i,k\}$ is determined by the sum of the transition rates to all the accessible final states. In this section, we study a closely related quantity which characterizes the complete relaxation to the bottom of the conduction band of a *single* electron with initial energy $E_{\rm in}$, initially placed in subband $\{m_{\rm in},i_{\rm in}\}$. This process involves cascades of transitions through all the available channels and it is characterized by the ''average global relaxation time Θ of a single electron'' by LO phonon emission to the lowest accessible energy state. The set of all the states involved by this process is called a class and, clearly, the energies of the states of a same class differ by a multiple of $\hbar\omega_{\rm LO}$. The following recurrence relation is used to evaluate the average time Θ:

$$\Theta(\mathcal{S})^{-1}=\sum_{\mathcal{C}}\left[\tau_{\mathcal{S}\rightarrow\mathcal{C}}+\Theta(\mathcal{C})\right]^{-1}, \tag{14}$$

where $\mathcal{S}$ stands for a state $\{m,i,k\}$ and $\mathcal{C}$ for all the states accessible by one LO phonon emission ($\mathcal{C}$ for ''child''). As we consider only LO phonon scattering, an electron with an energy below $\hbar\omega_{\rm LO}$ cannot decay further and has already reached its lowest state.

In Fig. 6, Θ is represented as a function of the initial energy of an electron placed in subband $\{m_{\rm in},i_{\rm in}\}$. The wire [case (b) of Fig. 2] has a subband separation of about 50 meV and the initial subbands are $\{0,1\}$ and $\{0,0\}$, respectively, in the upper and lower parts.

Two main quantities determine the general behavior of Θ: the number of ''steps'' (number of successive transitions) needed for complete decay $n_{\rm st}=\mathrm{int}(E_{\rm in}/\hbar\omega_{\rm LO})$ (here int denotes the integral part function) and the number of available relaxation channels $n_{\rm ch}$. $n_{\rm st}$ is incremented by one unit at each $\hbar\omega_{\rm LO}$ above the ground subband edge and $n_{\rm ch}$ at each $\hbar\omega_{\rm LO}$ above all other subband edges. Θ is a continuous monotonic increasing function of $E_{\rm in}$ in the initial energy interval where these two numbers are constant, because the transition rates are decreasing functions of the energy. Whenever $E_{\rm in}=E_{m,i}+n\hbar\omega_{\rm LO}$ [with n an integer and $(m,i)\neq(0,0)$], a new channel opens and Θ decreases discontinu-

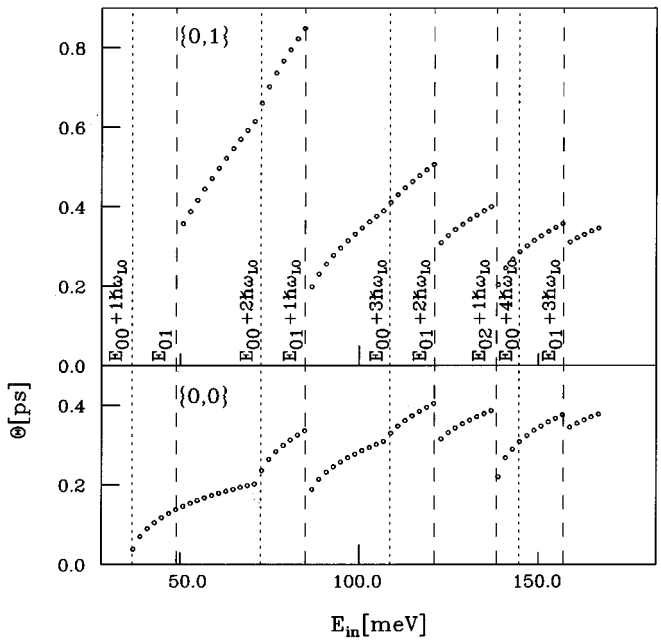

FIG. 6. Average global relaxation time Θ needed by a single electron of initial energy $E_{\rm in}$ placed in subbands $\{0,0\}$ (lower graph) and $\{0,1\}$ (upper graph) to reach the bottom of the conduction band by LO-phonon emission. The jumps (dashed vertical lines) are due to the divergences of the transition rates at the opening of new channels, i.e., at energies lying $n(\hbar\omega_{\rm LO})$ above an excited subband edge (n integer). The discontinuities of $d\Theta/dE_{\rm in}$ (dotted vertical lines) are due to the increase of the number of relaxation steps which occurs whenever the ground subband edge is $n(\hbar\omega_{\rm LO})$ below the initial energy. Comparing the upper and lower cases, no systematic tendency of the average behavior of $\Theta(E_{\rm in})$ to increase or decrease can be distinguished.

ously to a lower value (Fig. 6). This discontinuity is important because, when a new channel opens, the first available state is located at the final subband edge and the transition is necessarily associated with a divergent rate due to the 1D density of states. Each time a new step is added, a discontinuity of $d\Theta/dE_{\rm in}$ appears as clearly visible in Fig. 6.

Concerning the global trend, on the one hand Θ is lengthened with $E_{\rm in}$ due to the step number increase and the rate decrease, while on the other hand Θ is shortened by the opening of new channels. The competition between these processes does not allow any simple general tendency for Θ as a function of $E_{\rm in}$ to be recognized, as shown by the comparison of the two cases given in Fig. 6.

The mean value of Θ is remarkably small when $m_{\rm in}=0$. Even if the transition rates are smaller than for quantum wells, the time needed by electrons to cool down is shorter than for 2D structures, because the presence of different channels offers many ways for the electrons to relax. If the z quantum number has to change in order to reach the bottom of the conduction band, the basic value of Θ is more than one order of magnitude larger, as predicted by the rate analysis. For example, the average global relaxation time needed by an electron to decay from $\{1,0\}$ to the lowest accessible state amounts to $\simeq 10$ ps, while it is in the subpicosecond range for all initial subbands with z quantum number $m_{\rm in}=0$. This is not observed for the wider wire because the $\{1,0\}$ subband lies $\simeq\hbar\omega_{\rm LO}$ above the $\{0,2\}$ one.

C. Population relaxation dynamics

The above considerations do not take into account level population effects occurring when many electrons are decaying simultaneously in the system. To study such effects, we shall solve the rate equations (Boltzmann equation) related to an initial distribution of electrons in an excited subband and the dynamics of its decay. The equation of evolution of the populations is

$$\frac{dn_S(E,t)}{dt}=\sum_P \tau_{P\to S}^{-1}(E+\hbar\omega_{\rm LO})n_P(E+\hbar\omega_{\rm LO},t)\times[1-n_S(E,t)]\rho_P(E+\hbar\omega_{\rm LO})-\sum_C \tau_{S\to C}^{-1}(E)n_S(E,t)\times[1-n_C(E-\hbar\omega_{\rm LO},t)]\rho_C(E-\hbar\omega_{\rm LO}) \quad . \tag{15}$$

In this equation, $n_S(E,t)$ is the probability of finding an electron of energy E in subband S at time t; the first term on the rhs represents the filling from the parent states located in subbands P; the second term represents the emptying to children states in subbands C; $\tau_{S\to C}^{-1}(E)$ are the LO-phonon rates appearing in Eq. (11); $\rho_S(E)$ is the density of states in subband S.

We now assume that a Gaussian excitation, e.g., an optical pulse, provides in a unique high subband an initial population of electrons given by the ratio of the Gaussian to the density of states of the subband concerned.

The average energy $\langle E\rangle$, as well as the populations $n_S(E,t)$ in each subband, are computed at each step of the Runge-Kutta-Merson integration of Eq. (15). Like previously, the complete set of all the states can be divided into classes by grouping together those states whose energies differ by a multiple of $\hbar\omega_{\rm LO}$. Longitudinal optical scattering does not couple different classes which evolve independently.

In Figs. 7(a) and 7(b) we present the numerical results corresponding, respectively, to the two structures mentioned as (a) and (b) in Fig. 2. The figures (a) and (b) display in the lower part the average energy $\langle E\rangle$ as a function of time and in the upper parts the populations $n_S(E,t)$ in initial and final subbands. The case (ii) includes the effects of an additionnal phenomenological relaxation which will be discussed later. The present discussion relates to the evolution of the populations due to LO phonon emission only [case (i)]: the evolution of the population in the initial subband at time $t=0$ and at an early stage [$t=28$ fs for the case of Fig. 7(a) and $t=0.4$ ps for Fig. 7(b)] reveals discontinuities due to the rate singularities towards the subband edges $E_{m,i}$ [graph (i)]. It is also closely related to the discontinuous behavior of the lifetime of the states in the initial subband [obtained as the inverse of the sum of the rates $(\Sigma_{\rm fi}\tau_{\rm in\to fi}^{-1})^{-1}$] and it looks like a product of this lifetime and the initial population, as expected. On the low energy side of the same part of the graph is presented the asymptotic population in the final few subbands $\{m,i\}$ with $E_{m,i}<\hbar\omega_{\rm LO}$. It only extends over one optical phonon energy, as it should, and exhibits discontinuities corresponding to the different filling rates.

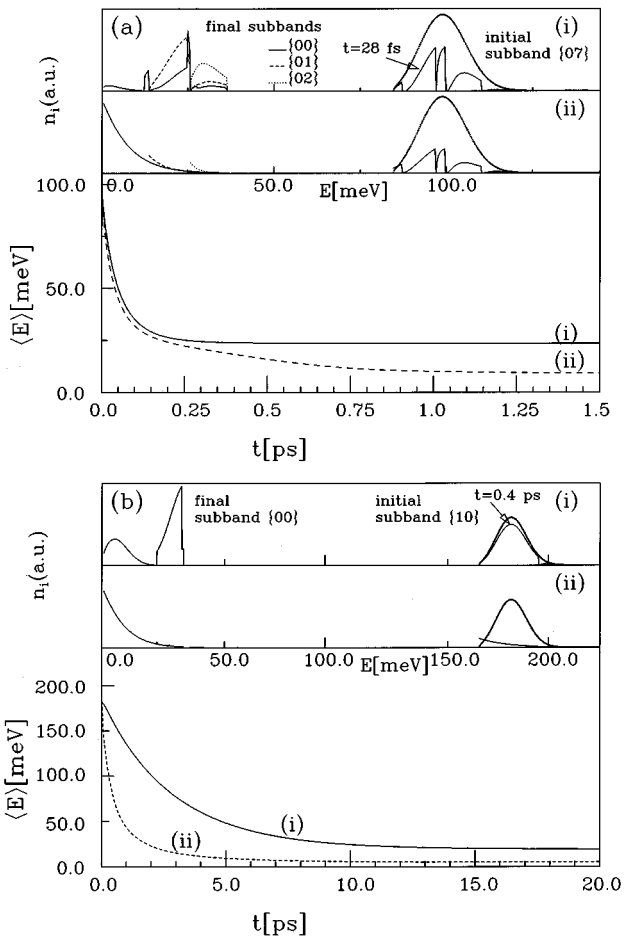

FIG. 7. Relaxation dynamics of an electron population initially placed in a high subband for the two cases of Fig. 2: (a) large wire, (b) small wire. The two upper graphs show the populations in selected subbands; the lower graph shows the average energy $\langle E \rangle$ as a function of time. The graph and the curve denoted by (i) refer to a decay exclusively due to LO phonon scattering, while for (ii) a phenomenological intrasubband thermalization is added. (a) The population of the initial subband $\{0,7\}$ at time $t=0$ ps and at an early stage ($t=28$ fs) is shown in the high energy side: the final population at $t=1.8$ ps in the lowest subbands is plotted in the low energy side. (b) The population of the initial subband $\{1,0\}$ is shown at times $t=0$ ps and $t=0.4$ ps: the final population at time $t=14.4$ ps [7.2 ps for the graph (ii)] only involves the subband $\{0,0\}$ since the splitting is greater than $\hbar\omega_{\mathrm{LO}}$.

In the case of a ''large'' wire [Fig. 7(a)], the initial subband is the eighth excited one: $E_{0,7}=84.5$ meV. The average energy shown in the lower part of the figure decreases quite fast and reaches after 0.4 ps its asymptotic value of 23.6 meV, corresponding to the energy of the asymptotic final population shown at $t=1.8$ ps in inset (i). This final population involves the subbands $\{0,0\}$ (solid line), $\{0,1\}$ (dashed line), and $\{0,2\}$ (dotted line) with respective subband edges $E_{0,0}=0.0$ meV, $E_{0,1}=13.6$ meV, and $E_{0,2}=25.6$ meV. The ordering of the rates according to the quantum numbers mentioned in Sec. III A is responsible for the structure of the final population: this population is predominant in the most excited available subband because it is easier for electrons to change their x quantum number by only one, as compared to several, units. Only a few electrons populate subband $\{1,0\}$ during the relaxation process since transitions from $m=0$ subbands to $m=1$ subbands have a small probability.

Figure 7(b) shows the same quantities as Fig. 7(a) for the small quantum wire, where the initial subband is now the fourth excited one, $\{1,0\}$, which differs from the lowest subband by the z quantum number. A slow relaxation process is observed, since the decay rate is much lower when the first z quantum number has to change in the process. The fewer available channels also affect this result since the typical level spacing now reaches 50 meV as shown in Fig. 2(b). The average energy relaxes in about 15 ps down to the asymptotic value of 18.8 meV [bottom of Fig. 7(b)]. The initial population decreases particularly slowly. We observe that once the electrons reach a subband with zero z quantum number, they join the bottom of the subband nearly as fast as for the large structure. Hence, the intermediate subband populations are always small. The final population in this case involves only the ground subband, since the first excited subband edge $E_{0,1}=56$ meV lies higher than $\hbar\omega_{\mathrm{LO}}$.

Finally let us consider, for both quantum wires (a) and (b), the effect of a fast phenomenological intrasubband thermalization. Such a phenomenon is present in all available experimental time-resolved measurements where one sees luminescence mainly issuing from the subband edges.[3,32,34,42–44] According to a simple theoretical argument, the two particle electron-electron Coulomb interaction is unable to provide kinetic energy redistribution in a strictly one-dimensional structure: conservation of both energy and momentum allows only a final pair state which is identical to the initial one.[4] The energetic broadening of the electronic states due to their finite lifetimes could slightly ''bend'' this rule. The investigation of other more complicated processes which could eventually explain a fast intrasubband relaxation lies beyond the scope of the present paper. Instead, we introduce a fast *phenomenological* intrasubband thermalization process conserving the number of particles and the total kinetic energy within a given subband. This is achieved by adding the following term to Eq. (15):

$$\frac{[n_S^0(E,\mu_S(t),T_S(t))-n_S(E,t)]}{\tau_{\mathrm{th}}}\ , \tag{16}$$

where $\tau_{\mathrm{th}}=70$ fs is the phenomenological thermalization time, $n_S^0(E,\mu_S(t),T_S(t))$ is the asymptotic equilibrium Fermi distribution function in subband S, $\mu_S(t)$ and $T_S(t)$ are the chemical potential and the temperature, respectively, and they are evaluated self-consistently at each step of the evolution from the knowledge of the number of particles and the total energy in each subband. The different classes now couple together, in opposition to what happened in the case without thermalization, since both μ_S and T_S depend on all the states belonging to the S subband. From the physical point of view, it is important to note that the expression (16) is not a diffusion or detailed balance term in k space as one might expect, but it is simply a term that forces the distribution of each subband to relax to an internal thermal equilibrium during a typical time scale τ_{th}. The introduction of this kind of term is justified since our aim is not to describe the unknown microscopic dynamics on the 10 fs time scale but

to obtain an insight into the possible accelerating effect of a fast intrasubband thermalization mechanism on the slower LO-phonon relaxation.

In Figs. 7(a) and 7(b) the curves and graphs including the effect of a fast intrasubband thermalization are labeled (ii). The lower parts of the figures show that the decay of the average energy is accelerated [dashed curves (ii)]. This effect is much more pronounced for the narrow wire where fewer channels are available. However, from this it cannot be deduced that the observed acceleration of the decay is universal, since one of the effects of the thermalization is to modify the feeding or emptying of the channels: if the thermalization feeds fast channels and empties slow channels it accelerates the decay, but the opposite could also happen with the opposite consequence. The two trends compete and the effect depends on the population. The final energy is clearly seen to be significantly lower in both examples of wires, since the second effect of fast intrasubband thermalization is to rearrange the low-lying subbands and feed upper levels for which LO-phonon transitions are allowed. The lowering of the average energy $\langle E \rangle$ lasts until the electron densities in all subbands become negligible for energies above $\hbar\omega_{\mathrm{LO}}$. In the case of the large wire [Fig. 7(a)], this seems to happen as a second phase in the relaxation process bringing the overall relaxation time up to 1 ps and the final energy down to 8.4 meV. Graph (ii) also shows that the predominance of the final population in the highest available excited subband is still present. In Fig. 7(b), the thermalization has a much stronger accelerating effect on the relaxation time: after 7.0 ps, the population can be considered as completely relaxed and the final energy is especially low (5.6 meV) since there is no trapping in higher subbands [graph (ii)]. Nevertheless the relaxation remains slower than in the larger wire.

IV. CONCLUSION

The LO-phonon mediated relaxation dynamics of hot electrons in weakly-one-dimensional quantum wires has been investigated. In a first step, the electronic states of a geometrically complex wire have been computed in the framework of the adiabatic approximation. This technique capitalizes on the smoothness of the curves describing the cross section of weakly-one-dimensional wires. The relaxation rates between any pair of LO-phonon coupled states were then evaluated using the Fermi golden rule, and an interpretation in terms of quantum numbers, allowed by the adiabatic approach, was presented. The single-electron total decay time was determined with respect to the initial excited state. The last section treated the investigation of the electron population dynamics for two different wires, large and small, with or without a phenomenological intrasubband thermalization.

We have shown that the relaxation rate functions are clearly ordered with respect to the quantum numbers of the states involved. As expected, the intrasubband relaxation is always the most rapid, i.e., the kinetic energy is quickly lost. For intersubband relaxation, the rates are smaller, but of the same order of magnitude, when the quantum number in the strongest confinement direction is preserved, and ordered with respect to the quantum number in the weak confinement direction. If the quantum number of the strong confinement direction is changed in the relaxation process, the transition rates are about one order of magnitude smaller.

The average global relaxation time needed by a single excited electron to reach the lowest accessible conduction band state presents discontinuities as a function of the initial electron energy, due to the divergence of the relaxation rate towards a subband edge at the opening of a new channel. Contrary to our first intuition, this time does not inevitably increase as a function of the initial energy because the number of available channels increases too. We observed that the average global relaxation time is less than a picosecond when the initial electron is in the ground state in the direction of strong confinement, but can be one order of magnitude greater otherwise.

The dynamics of an ensemble of excited electrons including level population effects has been investigated. The characteristic decay time can vary significantly, depending on the initial subband, the resonance conditions with LO phonons, and the dimensions of the wire. However, it is inevitably smaller in larger wires due to the larger number of available channels.

When a fast phenomenological intrasubband thermalization process is added, the populations rearrange rapidly to fit Fermi distributions in each subband. This process lowers the final energy and this lowering might appear as a second phase in the overall relaxation, especially in large wires. In small wires, the intrasubband thermalization may also significantly speed up the relaxation.

ACKNOWLEDGMENTS

The support of the Swiss National Science Foundation through Grant No. 20-37642.93 is gratefully acknowledged. One of us (C.A.) is grateful to Professor P. Erdős for fruitful conversations and a critical reading of the manuscript. One of us (U.B.) thanks the Swiss Federal Institute of Technology of Lausanne for financial support at the initial stage of the work.

APPENDIX: PONDERATED REDUCED MASS

The expression (5) of the ponderated reduced mass m_{mi} is derived directly from the three-dimensional Schrödinger equation

$$\left[-\frac{\hbar^2}{2}\nabla\frac{1}{m^*(x,z)}\nabla+V(x,z)\right]\chi_k^x(z)\phi_k(x)e^{iky} = E\chi_k^x(z)\phi_k(x)e^{iky}. \tag{A1}$$

Using the adiabatic approximation, the z-dependent part of the kinetic energy operator and the potential $V(x,z)$ are absorbed by the effective potential $V_{k,m}^{\mathrm{eff}}(x)$ and the function $\chi_k^x(z)$ becomes $\chi_{k,m}^x(z)$. Projecting on $\chi_{k,n}^x(z)$, the x-dependent part of the kinetic energy operator applied to the envelope function becomes

$$-\frac{\hbar^2}{2}\int dz\,\chi_{k,n}^x(z)^*\frac{\partial}{\partial x}\frac{1}{m^*(x,z)}\frac{\partial}{\partial x}\chi_{k,n}^x(z)\phi_k(x)e^{iky}. \tag{A2}$$

Owing to the slow x dependence of $\chi^x_{k,n}$ the x derivatives can be permuted with $\chi^x_{k,n}$. A local ponderated effective mass is defined as

$$m^{-1}_{k,n}(x)=\int dz\chi^x_{k,n}(z)^* m^{*-1}(x,z)\chi^x_{k,n}(z) \qquad \text{(A3)}$$

and only the kinetic symmetric term $d/dx\,[m_{k,n}(x)^{-1}d(\phi_k(x)e^{iky})/dx]$ is retained in the resulting Schrödinger equation, giving

$$\left[-\frac{\hbar^2}{2}\frac{1}{m_{k,n}(x)}\frac{d^2}{dy^2}-\frac{\hbar^2}{2}\frac{d}{dx}\frac{1}{m_{k,n}(x)}\frac{d}{dx}+V^{\text{eff}}_{k,n}(x)\right]\times\phi_k(x)e^{iky}=E\,\phi_k(x)e^{iky}. \qquad \text{(A4)}$$

Expanding to second order in k near $k=0$, the last two terms in the square brackets are then replaced by the energy of the band edge $E_{k=0,n,i}$ and $\phi_k(x)$ by the eigenfunction $\phi_{k=0,n,i}(x)$. Projection on $\phi_{k=0,n,j}(x)$ gives

$$-\frac{\hbar^2}{2}\frac{1}{m_{nj}}\frac{d^2}{dy^2}e^{iky}=(E-E_{k=0,n,j})e^{iky}, \qquad \text{(A5)}$$

where

$$m^{-1}_{nj}=\int dx\,\phi_{k=0,n,j}(x)^* m^{-1}_{k=0,n}(x)\,\phi_{k=0,n,j}(x). \qquad \text{(A6)}$$

This last expression is precisely Eq. (5).

[1] H. Sakaki, Jpn. J. Appl. Phys. **19**, L735 (1980).
[2] H. Sakaki, Surf. Sci. **267**, 623 (1992), and references therein.
[3] A. C. Maciel, C. Kiener, L. Rota, J. F. Ryan, U. Marti, D. Martin, F. Morier-Genoud, and F. K. Reinhart, Appl. Phys. Lett. **66**, 3039 (1995).
[4] J. P. Leburton, Phys. Rev. B **45**, 11 022 (1992).
[5] L. Rota, F. Rossi, S. M. Goodnick, P. Lugli, E. Molinari, and W. Porod, Phys. Rev. B **47**, 1632 (1993).
[6] L. Rota, F. Rossi, P. Lugli, and E. Molinari, Phys. Rev. B **52**, 5183 (1995).
[7] F. A. Riddoch and B. K. Ridley, Surf. Sci. **142**, 260 (1984).
[8] J. P. Leburton, J. Appl. Phys. **56**, 2850 (1984).
[9] S. Briggs and J. P. Leburton, Phys. Rev. B **38**, 8163 (1988).
[10] T. Yamada and J. Sone, Phys. Rev. B **40**, 6265 (1989).
[11] S. Briggs and J. P. Leburton, Phys. Rev. B **43**, 4785 (1991); J. P. Leburton, J. Appl. Phys. **74**, 1417 (1993).
[12] D. Jovanovic, S. Briggs, and J. P. Leburton, Phys. Rev. B **42**, 11 108 (1990).
[13] U. Bockelmann and G. Bastard, Phys. Rev. B **42**, 8947 (1990).
[14] M. A. Stroscio, Phys. Rev. B **40**, 6428 (1989); M. A. Stroscio, K. W. Kim, M. A. Littlejohn, and H. Chuang, *ibid.* **42**, 1488 (1991).
[15] K. W. Kim, M. A. Stroscio, A. Bhatt, R. Mickevicius, and V. V. Mitin, J. Appl. Phys. **70**, 319 (1991).
[16] S. R. Ren and Y. C. Chang, Phys. Rev. B **43**, 11 857 (1991).
[17] B. F. Zhu, Phys. Rev. B **44**, 1926 (1991).
[18] P. A. Knipp and T. L. Reinecke, Phys. Rev. B **45**, 9091 (1992).
[19] B. A. Foreman, Phys. Rev. B **52**, 12 260 (1995).
[20] W. Jiang and J. P. Leburton, J. Appl. Phys. **74**, 1652 (1993); **74**, 2097 (1993).
[21] F. Rossi, L. Rota, C. Bungaro, P. Lugli, and E. Molinari, Phys. Rev. B **47**, 1695 (1993).
[22] S. Briggs, B. A. Mason, and J. P. Leburton, Phys. Rev. B **40**, 12 001 (1989).
[23] V. B. Campos and S. Das Sarma, Phys. Rev. B **45**, 3898 (1992); V. B. Campos, S. Das Sarma, and M. A. Stroscio, *ibid.* **46**, 3849 (1992).
[24] L. Rota, J. F. Ryan, F. Rossi, P. Lugli, and E. Molinari, Europhys. Lett. **28**, 277 (1994).
[25] J. R. Senna and S. Das Sarma, Phys. Rev. B **48**, 4552 (1993).
[26] I. Vurgaftman, Y. Lam, and J. Singh, Phys. Rev. B **50**, 14 309 (1994).
[27] S. Yu, K. W. Kim, M. A. Stroscio, and G. J. Iafrate, Phys. Rev. B **51**, 4695 (1995).
[28] R. Mickevicius, V. Mitin, and V. Kochelap, J. Appl. Phys. **77**, 5095 (1995).
[29] P. A. Knipp and T. L. Reinecke, Phys. Rev. B **52**, 5923 (1995).
[30] E. Kapon, D. M. Hwang, and R. Bhat, Phys. Rev. Lett. **63**, 430 (1989).
[31] G. Bastard, J. A. Brum, and R. Ferreira, in *Solid State Physics: Advances in Research and Applications*, edited by H. Ehrenreich and D. Turnbull (Academic Press, New York, 1991), Vol. 44, p. 229.
[32] M. Grundmann, J. Christen, M. Joschko, O. Stier, D. Bimberg, and E. Kapon, Semicond. Sci. Technol. **9**, 1939 (1994).
[33] I. Vurgaftman and J. Singh, Appl. Phys. Lett. **62**, 2251 (1993).
[34] C. Kiener, L. Rota, K. Turner, J. M. Freyland, A. C. Maciel, and J. F. Ryan (unpublished); J. F. Ryan, A. C. Maciel, C. Kiener, L. Rota, K. Turner, J. M. Freyland, U. Marti, D. Martin, F. Morier-Gemoud, and F. K. Reinhart, Phys. Rev. B **53**, R4225 (1996).
[35] G. Bastard, *Wave Mechanics Applied to Semiconductor Heterostructures* (Les Editions de Physique, Paris, 1990).
[36] D. Y. Oberli, F. Vouilloz, M.-A. Dupertuis, C. Fall, and E. Kapon, Il Nuovo Cimento **17D**, 1641 (1995).
[37] C. R. Bennett, N. C. Constantinou, M. Babiker, and B. K. Ridley, J. Phys. Condens. Matter **7**, 9819 (1995).
[38] R. Ferreira and G. Bastard, Phys. Rev. B **40**, 1074 (1989).
[39] M. C. Tatham, J. F. Ryan, and C. T. Foxon, Phys. Rev. Lett. **63**, 1637 (1989).
[40] K. Turner, L. Rota, R. A. Taylor, J. F. Ryan, and C. T. Foxon, Appl. Phys. Lett. **66**, 3188 (1995).
[41] M. Hartig, S. Haacke, B. Deveaud, and L. Rota (unpublished).
[42] H. Akiyama *et al.*, Phys. Rev. Lett. **72**, 924 (1994).
[43] S. Haacke, M. Hartig, D. Y. Oberli, B. Deveaud, E. Kapon, U. Marti, and F. K. Rheinart, Solid-State Electron. **40** (1-8 Special Issue S1), 299 (1996).
[44] R. Cingolani, H. Lage, L. Tapfer, H. Kalt, D. Heitmann, and K. Ploog, Phys. Rev. Lett. **67**, 891 (1991).